J. Fluid Mech. (2005), *vol.* 525, *pp.* 237–261.
DOI: 10.1017/S0022112004002733 Printed in the United Kingdom

Analysis and modelling of the temperature variance equation in turbulent natural convection for low-Prandtl-number fluids

By I. OTIĆ[1], G. GRÖTZBACH[1] AND M. WÖRNER[2]

[1]Forschungszentrum Karlsruhe, Institute for Nuclear and Energy Technologies, PO Box 3640, 76021 Karlsruhe, Germany

[2]Forschungszentrum Karlsruhe, Institute for Reactor Safety, PO Box 3640, 76021 Karlsruhe, Germany

(Received 27 January 2004 and in revised form 6 October 2004)

Results of direct numerical simulation (DNS) for Rayleigh–Bénard convection for the Prandtl number $Pr = 0.025$ are used to show some peculiarities of turbulent natural convection for low-Prandtl-number fluids. Simulations for this flow at sufficiently large Rayleigh numbers became feasible only recently because this flow requires the resolution of very small velocity scales and the recording of long-wave structures for the slow changes in the convective temperature field. The results are used to analyse standard turbulent heat flux models. The analysis for a model based on the Reynolds analogy indicates strong deficiencies of such turbulent heat flux models for low-Prandtl-number fluids. Turbulence models for buoyant flows which are not based on the Reynolds analogy include also the transport equation for the temperature variance $\overline{\theta^2}$. Detailed analysis of this transport equation and of the transport equation for the temperature variance dissipation rate is performed using DNS data. The results show the relevance of the turbulent diffusion terms and strong quantitative and qualitative deficiencies of standard models for turbulent diffusion of the temperature variance $\overline{\theta^2}$ and for the turbulent diffusion of the temperature variance dissipation rate ϵ_θ. Using the two-point correlation technique, statistical turbulence models for the turbulent diffusion of the temperature variance and for the turbulent diffusion of the temperature variance dissipation rate are proposed. These new models explicitly consider the molecular fluid properties. The new models reproduce the DNS results for $Pr = 0.025$ and $Pr = 0.71$ sufficiently well.

1. Introduction

Owing to the specific properties of many low-Prandtl-number fluids such as liquid metals, the experimental thermal and hydraulic investigations at the present stage are rather limited. For example, we have currently no sensors for accurate measurements of the small-scale velocity fluctuations, which are needed to determine accurately the local turbulent heat fluxes in liquid lead–bismuth. Therefore, numerical investigations by means of direct numerical simulation (DNS) are necessary in order to understand the physical mechanisms of turbulent convection in liquid metals and to gain some of the required turbulence data.

Most of the common turbulent heat flux models use the simple concept of the Reynolds analogy based on a turbulent Prandtl number (Pr_t) to model the turbulent heat transfer. This concept is, in general, problematic as Pr_t depends in an unknown manner on many flow and fluid parameters (see e.g. Kays 1994). To obtain more

realistic predictions for the convective turbulent heat transfer, models are required, which are based on the transport equations for the turbulent heat flux and for the temperature variance. The buoyancy term in the heat flux equations includes the temperature variance $\overline{\theta^2}$. In analogy to the turbulent kinetic energy k, the temperature variance $\overline{\theta^2}$ is a measure for the temperature fluctuations. Launder (1988) simplifies the heat flux equations and suggests the following algebraic heat flux model:

$$\overline{u_i\theta} = -C_1\tau\left[\overline{u_iu_j}\frac{\partial\overline{T}}{\partial x_j} + C_2\overline{u_j\theta}\frac{\partial\overline{U_i}}{\partial x_j} + C_3\beta g_i\overline{\theta^2}\right], \tag{1.1}$$

where $U_i = \overline{U_i} + u_i$ and $T = \overline{T} + \theta$ denote the Reynolds decomposition of velocity and temperature. C_1, C_2, C_3 are empirical coefficients, g is gravity, β the thermal expansion coefficient, and τ is a characteristic time scale of the turbulent heat transfer. Usually, τ is given as the mechanical time scale k/ϵ, where k is the turbulent kinetic energy and ϵ the dissipation rate of k. The Reynolds stress tensor $\overline{u_iu_j}$ is usually modelled by means of an eddy viscosity ansatz using transport equations for k and ϵ or by the modelled transport equations for the Reynolds stress tensor.

These equations contain several terms which can hardly be measured, but have to be modelled, such as the temperature variance dissipation rate. DNS is a tool which can provide such data and complement the experimental studies as, for example, the ongoing project in the Karlsruhe lead laboratory (KALLA) (see Knebel *et al.* 2001) on thermal and hydraulic investigations in liquid lead–bismuth ($Pr \sim 0.025$).

In this paper, we will use DNS to investigate some peculiarities of the natural convection process in a fluid with $Pr = 0.025$ and to analyse some relevant statistical turbulence data. The results show the relevance of the turbulent diffusion terms and strong quantitative and qualitative deficiencies of standard models for the turbulent diffusion of the temperature variance $\overline{\theta^2}$ and for the turbulent diffusion of the temperature variance dissipation rate ϵ_θ. The two-point correlation technique first introduced by Chou (1945) and Burgers (1953) and subsequently applied and extended by Kolovandin & Vatutin (1972) and more recently by Jovanović, Ye & Durst (1995) forms the basis of our theoretical approach. The results of this approach are new statistical models for the turbulent diffusion terms in the transport equations for the temperature variance $\overline{\theta^2}$ and for the temperature variance dissipation rate ϵ_θ. These models account for the peculiarities of the turbulent natural convection in low-Prandtl-number fluids and lead therefore to an increased accuracy of turbulent heat flux models.

2. Problem specification and method of solution

A simple physical model for the investigation of heat transfer by natural convection is the Rayleigh–Bénard convection. It is given by an infinite fluid layer which is confined by two rigid horizontal isothermal walls. The lower one is heated and the upper one is cooled. The physical problem is characterized by two dimensionless numbers: The Rayleigh number

$$Ra = \frac{g\beta\Delta T D^3}{\nu\kappa},$$

and the Prandtl number

$$Pr = \frac{\nu}{\kappa},$$

where g is gravity and β the thermal expansion coefficient as introduced above, ΔT is the wall temperature difference, D is the distance between the two horizontal walls,

ν is the kinematic viscosity and κ is the thermal diffusivity. An alternative to one of the dimensionless numbers above is the Grashof number

$$Gr = \frac{Ra}{Pr}.$$

2.1. *DNS of Rayleigh–Bénard convection*

Direct numerical simulation is a method in which the three-dimensional conservation equations for mass, momentum and energy are solved numerically such that all relevant physical processes are resolved by the grid and by the computational domain. This means that the mesh size is fine enough to resolve the smallest scales of turbulence and to resolve the viscous and thermal boundary layers in the near-wall region. In particular, the periodicity lengths which define the size of the computational domain must be large enough to resolve the largest scales of turbulence. Meeting both requirements determines the computational effort for such DNS, especially for convection in liquid metals.

Simulations of Rayleigh–Bénard convection are performed with the TURBIT code (Grötzbach 1987; Wörner 1994). It is a finite volume code which allows for direct numerical simulations of turbulent heat and mass transfer in simple channel geometries. The governing equations for mass, momentum and energy are solved in dimensionless form where the following normalization is used: channel height D, velocity $u_0 = \sqrt{g\beta\Delta T D}$, time D/u_0, pressure ρu_0^2, and difference between the temperatures of the two walls ΔT. For spatial discretization a staggered grid and second-order central finite differences are used. Time integration of the momentum equation is performed by the explicit Euler–Leapfrog scheme, involving the projection method of Chorin. For time integration of the energy equation, the semi-implicit Leapfrog–Crank–Nicholson scheme is used. The boundary conditions use periodicity in both horizontal directions, whereas at the lower and upper wall the no-slip condition and constant wall temperatures are specified. Owing to above normalization, the Reynolds number is given as $Re_0 = u_0 D/\nu$ and it follows $Re_0 = \sqrt{Gr_0}$. Here, X_1, X_2 denote horizontal directions and X_3 the vertical direction. N_1, N_2 denote the number of mesh cells in horizontal directions, and N_3 the number of mesh cells in the vertical direction. L_i denote the lengths of the computational domain.

In the following analysis, we will use data from a new DNS, but also data from former simulations of Rayleigh–Bénard convection, for $Pr = 0.71$ in the turbulent regime, and those for $Pr = 0.006$ in the turbulent but mainly conductive regime by Wörner (1994). The objective for the new simulation at $Pr = 0.025$ is to find the parameter range in which the heat transfer is more strongly governed by turbulent convection. This simulation is started from an earlier simulation by Bunk & Wörner (1998) with the same Prandtl number and lower Rayleigh number. The results of the earlier simulation are interpolated to the finer grid and advanced in time. It is characterized by $Ra = 100\,000$ and is performed on a mesh with $400 \times 400 \times 75$ cells within the horizontally periodic domain of size $8 \times 8 \times 1$ (see table 1). This periodic domain was selected according to numerical studies for low-Prandtl-number Rayleigh–Bénard convection by Wörner (1994). One-dimensional energy spectra and autocorrelations of velocity and temperature fluctuations are evaluated, indicating that small and large scales of turbulence are well resolved within this computational domain. However, the velocity autocorrelation in the X_1-direction at large distances deviates slightly from zero indicating that a smaller computational domain (than $8 \times 8 \times 1$) may be insufficient to resolve large scales of the velocity field at these Rayleigh and Prandtl numbers. After some simulation time to reach a statistically fully

Pr	Ra	Re_0	$L_{1,2}$	$N_{1,2}$	N_3
0.71	630 000	941.9	7.92	200	49
0.025	100 000	2000	8	400	75
0.006	24 000	2000	8	250	49

TABLE 1. Parameters of the simulations.

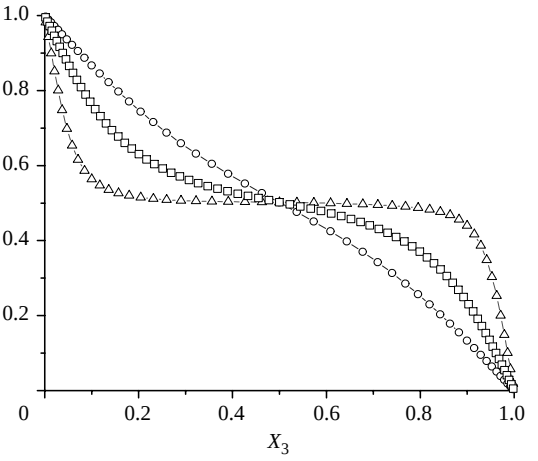

FIGURE 1. Mean temperature profiles for ○, $Pr = 0.006$, $Ra = 24\,000$; □, $Pr = 0.025$, $Ra = 100\,000$; △, $Pr = 0.71$, $Ra = 630\,000$.

developed convection state, the simulation covers about 18 000 statistically relevant time steps for analysing the results. In the following, we assign a time-averaged quantity with $\overline{X}$. Numerically, $\overline{X}$ is determined by averaging the data over both homogeneous horizontal directions and over time.

2.2. *Numerical results*

To point out the effect of the large thermal diffusivity, i.e. of the small Prandtl number, we compare the mean temperature profiles of the above referenced DNS results for Rayleigh–Bénard convection at $Pr = 0.006$ and $Pr = 0.71$ with the new results for $Pr = 0.025$ (figure 1). The simulations are carried out at similar Grashof numbers of about $10^6 - 4 \times 10^6$ which means these flows have similar turbulence scales in the velocity fields. The mean temperature profiles differ significantly, depending on the Prandtl number. For $Pr = 0.71$ ($Pr \sim 0.71$ corresponds, for example, to air), we find a constant plateau in the channel central region and thin thermal boundary layers. For $Pr = 0.025$ ($Pr \sim 0.025$ corresponds, for example, to liquid lead–bismuth), we find very thick thermal boundary layers, so convection has a small influence on the heat transfer; thus, the Rayleigh number is obviously still not large enough to build up an area with a constant temperature in the middle of the channel. For $Pr = 0.006$ ($Pr \sim 0.006$ corresponds, for example, to sodium), there is an almost linear mean temperature profile with a boundary layer extending almost over the whole channel. This means that convection has very little influence on the vertical heat transfer at this Rayleigh number. Nevertheless, this case also has, like the others, a highly turbulent velocity field. In the following, we discuss some physical phenomena using the results of the recent DNS of the Rayleigh–Bénard convection for $Pr = 0.025$. Owing to

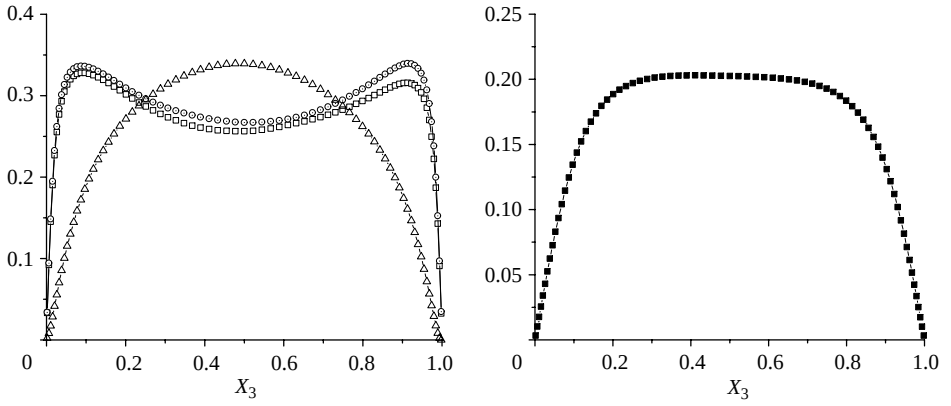

FIGURE 2. Vertical profiles of RMS values for $Pr = 0.025$, $Ra = 10^5$; □, u_1-RMS; ○, u_2-RMS; △, u_3-RMS; ■, θ-RMS.

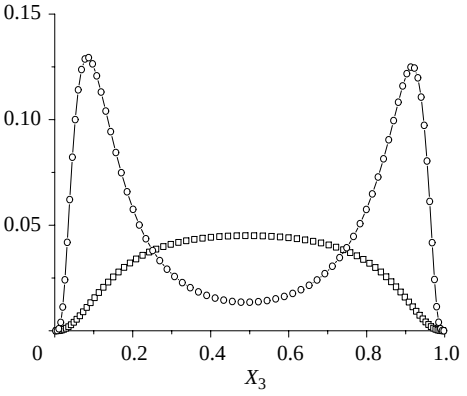

FIGURE 3. □, DNS evaluated profile of $\overline{u_3\theta}$; ○, DNS based results of the '$k-\epsilon-Pr_t$' model, ○, for $Pr = 0.025$, $Ra = 10^5$.

the large thermal diffusivity in comparison to the kinematic viscosity, temperature fluctuations are rapidly damped so that large structures dominate the temperature field, (see figure 1). Statistical quantities of the velocity and temperature fields, like the vertical profiles of the root-mean-square (RMS) values of the fluctuations, differ from each other strongly as well (see figure 2). For example, the form of the θ-RMS profile is not similar to any of the u_i-RMS profiles. In addition, the temperature fluctuation profile shows only one broad maximum; it is expected that, with higher Rayleigh numbers, two maxima will be formed with a local minimum in the middle. Figures 1 and 2 show that different scales exist in the temperature and velocity fields. Thus, assuming temperature and velocity fields and their statistical quantities to be similar in order to model the turbulent heat fluxes, as is done by assuming the Reynolds analogy in the turbulent Prandtl number (Pr_t) models, will necessarily lead to unsatisfactory predictions in the case of low-Prandtl-number flows. Figure 3 emphasizes this conclusion. Here, the standard parameters $Pr_t = 0.9$ and $c_\mu = 0.09$ were used in the modelled equations to calculate from the DNS data the vertical turbulent heat flux which would be predicted by the widely used $k-\epsilon-Pr_t$ model. These striking qualitative and quantitative differences may explain why these standard

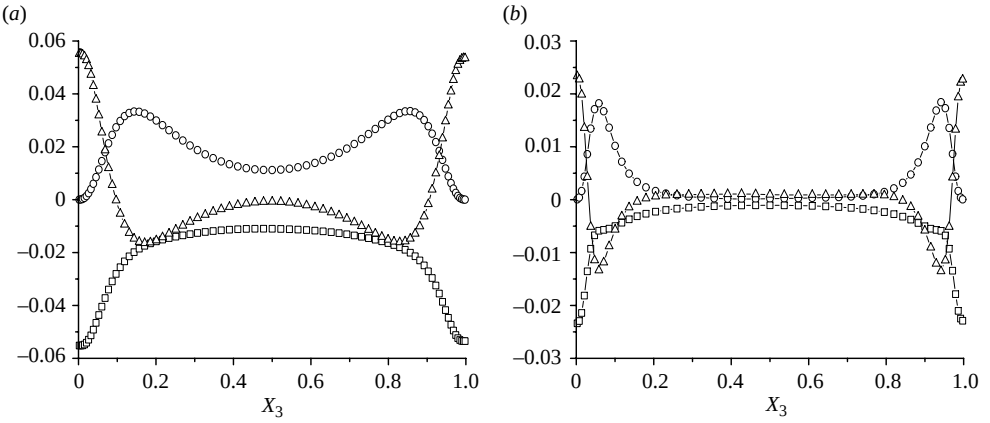

FIGURE 4. Vertical profiles of ○, P_θ; △, D_θ; and □, ϵ_θ in equation (3.1), for (*a*) $Pr = 0.025$ and (*b*) 0.71.

models quantitatively fail in this type of flow. Therefore it is desirable to develop a turbulence model which does not make use of the analogy between temperature and velocity fields. The model which accounts better for the characteristics of the turbulent convection in low-Prandtl-number fluids should be based on transport equations for the heat fluxes, for the temperature variance, and for the temperature variance dissipation rate, or at least on simplified algebraic forms of these equations.

3. Temperature variance

3.1. *Analysis of terms in the transport equation for the temperature variance*

The transport equation for the temperature variance $\overline{\theta^2}$ can be derived from the energy equation:

$$\frac{\partial \overline{\theta^2}}{\partial t} + \overline{U_i}\frac{\partial \overline{\theta^2}}{\partial x_i} = \underbrace{\underbrace{-\frac{\partial}{\partial x_i}\overline{u_i\theta^2}}_{D_\theta^t} + \underbrace{\kappa\frac{\partial^2\overline{\theta^2}}{\partial x_i \partial x_i}}_{D_\theta^m}}_{D_\theta} \underbrace{-2\overline{u_i\theta}\frac{\partial \overline{T}}{\partial x_i}}_{P_\theta} \underbrace{-2\kappa\overline{\frac{\partial\theta}{\partial x_i}\frac{\partial\theta}{\partial x_i}}}_{\epsilon_\theta}. \tag{3.1}$$

Since the mean velocities averaged over long times are zero in the turbulent Rayleigh–Bénard convection, there is no convective term in the transport equation for the temperature variance in the case of Rayleigh–Bénard convection. Figure 4 shows the budget of the transport equation (3.1) evaluated from the DNS data for $Pr = 0.025$ and $Pr = 0.71$. The turbulent heat fluxes $\overline{u_i\theta}$ are zero at the walls, therefore the production term P_θ is also zero. Since the mean temperature is nearly constant in the region outside of the thermal boundary layers for $Pr = 0.71$ at $Ra = 630\,000$ (see figure 1), P_θ is almost zero in this region. D_θ is usually interpreted as a diffusion term and it turns out to be of great importance in the flow considered. In the region very close to the walls, it is the diffusion term that balances the dissipation ϵ_θ. At the edges of the boundary layers, D_θ changes sign and largely contributes to the balance of the production term P_θ. Moreover, for higher turbulence intensities the term D_θ changes sign again to become slightly positive in the region outside the thermal boundary layers and balances the dissipation rate ϵ_θ (figure 4*b*). DNS of natural convection in a vertical channel was performed by Boudjemadi *et al.* (1996) for $Ra = 10^5$, $Pr = 0.71$,

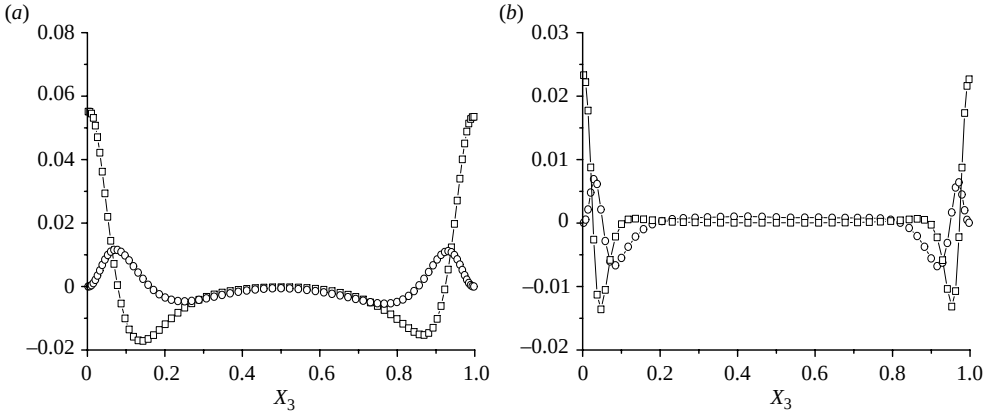

FIGURE 5. Vertical profiles of □, D_θ^m and ○, D_θ^t at (*a*) $Pr = 0.025$ and (*b*) 0.71.

and Versteegh & Nieuwstadt (1998) for $Ra = 5 \times 10^6$, $Pr = 0.709$. Evaluated budgets of the temperature variance in Boudjemadi *et al.* (1996) and Versteegh & Nieuwstadt (1998) show qualitatively the same behaviour of P_θ, D_θ and ϵ_θ compared to the results given in figure 4(*b*). Figures 5(*a*) and 5(*b*) show the contribution of the molecular diffusion D_θ^m and of the turbulent diffusion D_θ^t to D_θ. Near the walls, D_θ^m is one of the dominant terms in the budget of $\overline{\theta^2}$. A similar analysis of DNS data for $Pr = 0.006$ and $Ra = 24\,000$ is performed by Wörner & Grötzbach (1996*b*).

The closure of equation (3.1) requires modelling of the terms D_θ^t and ϵ_θ. First, we discuss D_θ^t. The closure of ϵ_θ will be discussed in § 4.

3.2. *Turbulent diffusion D_θ^t in the temperature variance equation*

3.2.1. *Analysis of existing D_θ^t models*

The triple correlation $\overline{u_i\theta^2}$ is usually modelled using a generalized gradient diffusion hypothesis (GGDH), first introduced by Daly & Harlow (1970), as

$$\overline{u_i\theta^2} = -C_{D\theta}\frac{k}{\epsilon}\overline{u_iu_j}\frac{\partial\overline{\theta^2}}{\partial x_j}, \tag{3.2}$$

or when replacing the tensor $(k/\epsilon)\overline{u_iu_j}$ by the scalar form k^2/ϵ by

$$\overline{u_i\theta^2} = -C_{S\theta}\frac{k^2}{\epsilon}\frac{\partial\overline{\theta^2}}{\partial x_i}, \tag{3.3}$$

as suggested by Spalding (1971). We use standard coefficients $C_{D\theta} = 0.22$, after Jones & Musonge (1988), and $C_{S\theta} = 0.3$ after Spalding (1971). Considering the time scale of the temperature field, instead of the velocity time scale, may improve the modelling, in particular for buoyant flows. This consideration gives the following gradient diffusion model

$$\overline{u_i\theta^2} = -C_{H\theta}\frac{\overline{\theta^2}}{\epsilon_\theta}\overline{u_iu_j}\frac{\partial\overline{\theta^2}}{\partial x_j}, \tag{3.4}$$

as used by Elghobashi & Launder (1983). $C_{H\theta} = 0.37$ will be used for comparisons. Taking into account the zero-fourth-order cumulant hypothesis of Milionshtchikov (1941) and neglecting most of the terms containing derivatives of the third moments in the transport equations for the triple velocity correlation, Hanjalić & Launder

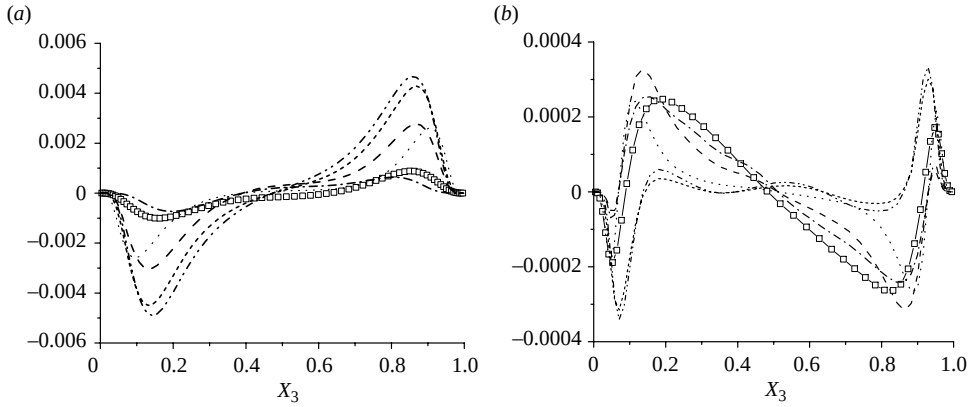

FIGURE 6. □, Comparison of DNS results for $\overline{u_3\theta^2}$, and DNS based results for $\overline{u_3\theta^2}$ as predicted by the equations (3.2) – – –, (3.3) ···, (3.4) - · -, (3.5) - · · - and (3.6) - - - for (*a*) $Pr = 0.025$, (*b*) 0.71.

(1972) derived an algebraic model for $\overline{u_iu_ju_k}$. Analogously, an algebraic model for $\overline{u_i\theta^2}$ may be given by

$$\overline{u_i\theta^2} = -C_{HL}\frac{k}{\epsilon}\left(\overline{u_iu_j}\frac{\partial\overline{\theta^2}}{\partial x_j} + 2\overline{u_j\theta}\frac{\partial\overline{u_i\theta}}{\partial x_j}\right), \tag{3.5}$$

as suggested by Deardorf (1973). Hanjalić & Launder (1972) take the coefficient in the model for $\overline{u_iu_ju_k}$ as $C_{HL} = 0.08$ and in their second paper (Hanjalić & Launder 1976) they propose $C_{HL} = 0.11$. For comparison with DNS data of the natural convection in a vertical channel, Dol, Hanjalić & Kenjereš (1997) choose $C_{HL} = 0.11$ in (3.5). We make the comparison using $C_{HL} = 0.08$. Dol, Hanjalić & Versteegh (1999) included the modelled production of the triple correlation in the model (3.5) to obtain

$$\overline{u_i\theta^2} = -C_{DHV}\frac{k}{\epsilon}\left(\overline{u_iu_j}\frac{\partial\overline{\theta^2}}{\partial x_j} + 2\overline{u_j\theta}\frac{\partial\overline{u_i\theta}}{\partial x_j} + 2\overline{u_iu_j\theta}\frac{\partial\overline{T}}{\partial x_j}\right), \tag{3.6}$$

where $\overline{u_iu_j\theta}$ is modelled by

$$\overline{u_iu_j\theta} = -C'\frac{k}{\epsilon}\left(\overline{u_iu_k}\frac{\partial\overline{u_j\theta}}{\partial x_k} + \overline{u_ju_k}\frac{\partial\overline{u_i\theta}}{\partial x_k}\right).$$

We take $C_{DHV} = 0.05$ after Dol *et al.* (1999). Figure 6 shows the comparison of vertical profiles of $\overline{u_i\theta^2}$ as evaluated from DNS and predictions of $\overline{u_i\theta^2}$ by the models (3.2), (3.3), (3.4), (3.5) and (3.6) for the case of Rayleigh–Bénard convection at $Ra = 1\times10^5$, $Pr = 0.025$ and at $Ra = 6.3\times10^5$, $Pr = 0.71$. Using a thermal time scale or some combination of thermal and mechanical time scales may improve the modelling of the turbulent heat transport, particularly in buoyancy dominated flows, but there is little evidence in support of this, mainly because most reported tests were performed for equilibrium flows where the ratio of the time scales does not vary appreciably, as pointed out by Hanjalić (1994). Figure 7 shows thermal and mechanical time scales for the cases of Rayleigh–Bénard convection for $Pr = 0.025$, $Ra = 1\times10^5$ and for $Pr = 0.71$, $Ra = 6.3\times10^5$ as evaluated from DNS. Figure 8 shows the vertical variation of the thermal to mechanical time scale ratio $\mathscr{R} = (\overline{\theta^2}/\epsilon_\theta)(\epsilon/k)$ for the cases considered. The thermal time scale in the considered parameter range is strongly

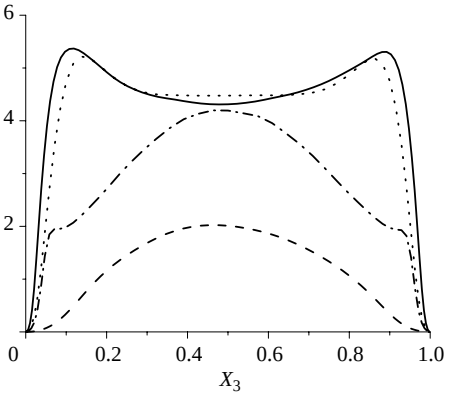

FIGURE 7. Vertical profiles of k/ϵ for the case of $Pr = 0.025$ $\cdots$ and $Pr = 0.71$ —, and vertical profiles of $\overline{\theta^2}/\epsilon_\theta$ for the case of $Pr = 0.025$ – – – and $Pr = 0.71$ - · -.

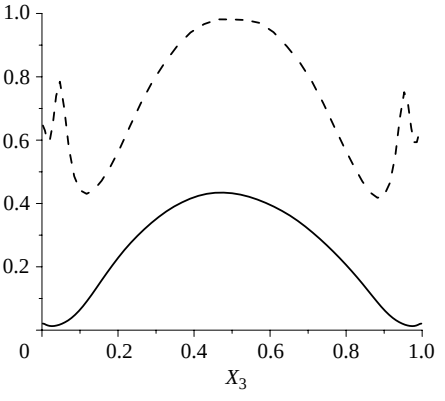

FIGURE 8. Vertical profiles of the time scale ratio $\mathscr{R}$, for the case $Pr = 0.025$ — and $Pr = 0.71$ – – –.

dependent on the flow parameters and position, so that this strong dependency also occurs in $\mathscr{R}$.

Comparing the prediction of $\overline{u_i\theta^2}$ which considers the thermal time scale in the gradient diffusion model type (equation (3.4)) with the DNS results for the case of $Pr = 0.71$ (figure 6*b*), we see the improvement of the GGDH model (equation (3.2)) at the edge of the thermal boundary layer and in the channel centre. In the near-wall region, both models give very similar values of $\overline{u_i\theta^2}$ but they are too low. Dol *et al.* (1997) evaluated DNS results of Versteegh & Nieuwstadt (1998) for an infinite differentially heated vertical channel at $Pr = 0.709$, $Ra = 5.4 \times 10^5$ and showed a similar improvement when using the thermal time scale with the gradient diffusion model. The coefficient used by Dol *et al.* (1997) was $C_{H\theta} = 0.22$. Comparing predictions by the model (3.4) with the experimental results of LaRue & Libby (1981) for the thermal mixing layer downstream of a half heated grid, Elghobashi & Launder (1983) found good agreement using the coefficient $C_{H\theta} = 0.35$ which is similar to the best fit $C_{H\theta} = 0.37$ we obtain for the Rayleigh–Bénard convection at $Pr = 0.71$, $Ra = 6.3 \times 10^5$.

Owing to the large thermal diffusivity compared to the kinematic viscosity of low-Prandtl-number fluids, the temperature fluctuations are damped strongly to give

a thermal time scale which may be very small. Comparing thermal time scales for $Pr = 0.025$ and for $Pr = 0.71$ (figure 7) as evaluated from DNS, we note that the thermal time scale for the case of $Pr = 0.025$ is about twice as low as the thermal time scale for $Pr = 0.71$ in the channel centre at these Rayleigh numbers. However, within the thermal boundary layers, the thermal time scales differ up to two orders of magnitude, where the mechanical time scales are still quite similar. This results in predictions by model (3.4) which are considerably lower, in particular in the region closer to the wall, than the DNS results, giving incorrect positions of the extremal points (figure 6*a*). No optimization of the coefficient $C_{H\theta}$ can improve this deficiency.

Comparison of the predictions of $\overline{u_i\theta^2}$ which consider the mechanical time scale, as given by the models (3.2), (3.3), (3.5) and (3.6), with DNS results show good optimization of the coefficients and fairly good agreement qualitatively and quantitatively for the case of $Pr = 0.71$ (figure 6*b*). However, obvious deficiencies of these models are still present when the gradient of $\overline{u_i\theta^2}$ is taken. This point will be discussed extensively later. Considering the same coefficients in the models (3.2), (3.3), (3.5) and (3.6) results in a strong overprediction for the case of $Pr = 0.025$ (figure 6*a*). Therefore, satisfactory predictions for both cases just by optimization of the constant coefficient, are obviously not possible.

Replacing the mechanical time scale by the thermal time scale in equations (3.3), (3.5) and (3.6) will result in predictions with displaced extrema for the case $Pr = 0.025$, as shown above for the GGDH model type.

This analysis indicates the following conclusions for modelling of the triple correlation vector $\overline{u_i\theta^2}$ which can cover a wide range of low Prandtl numbers:

(i) Simple modelling of the turbulent diffusion in the temperature variance equation requires explicit consideration of the influence of the molecular fluid properties.

(ii) Adequate modelling of the triple correlation vector $\overline{u_i\theta^2}$ seems to require the use of both, the mechanical and the thermal turbulence time scale.

(iii) The modelling of the turbulent diffusion, currently expressed in terms of a gradient of the transported quantity, possibly requires a new formulation, as pointed out by Hanjalić (1994).

3.2.2. *Development and analysis of a new model for* D_θ^t

In the following, we develop a new formulation for modelling of the turbulent diffusion in the temperature variance equation using the two-point correlation technique first introduced by Chou (1945) and Burgers (1953). Let a new coordinate system relative to two arbitrary points A and B be defined as

$$\xi_k = (x_k)_B - (x_k)_A, \tag{3.7}$$

$$(x_k)_{AB} = \tfrac{1}{2}[(x_k)_A + (x_k)_B]. \tag{3.8}$$

The differential operators at points A and B as functions of $(x_k)_{AB}$ and ξ_k are given as follows

$$\left(\frac{\partial}{\partial x_k}\right)_A = \left(\frac{\partial}{\partial x_k}\right)_{AB} \frac{\partial (x_k)_{AB}}{\partial (x_k)_A} + \frac{\partial}{\partial \xi_k}\frac{\partial \xi_k}{\partial (x_k)_A} = \frac{1}{2}\left(\frac{\partial}{\partial x_k}\right)_{AB} - \frac{\partial}{\partial \xi_k}, \tag{3.9}$$

$$\left(\frac{\partial}{\partial x_k}\right)_B = \left(\frac{\partial}{\partial x_k}\right)_{AB} \frac{\partial (x_k)_{AB}}{\partial (x_k)_B} + \frac{\partial}{\partial \xi_k}\frac{\partial \xi_k}{\partial (x_k)_B} = \frac{1}{2}\left(\frac{\partial}{\partial x_k}\right)_{AB} + \frac{\partial}{\partial \xi_k}. \tag{3.10}$$

From these two equations, we obtain

$$\left(\frac{\partial}{\partial x_k}\right)_A \left(\frac{\partial}{\partial x_k}\right)_B = \frac{1}{4}\left(\frac{\partial^2}{\partial x_k \partial x_k}\right)_{AB} - \frac{\partial^2}{\partial \xi_k \partial \xi_k}. \tag{3.11}$$

These results are known from (Hinze 1975, chap. 4-3). Applying the operator (3.11) to the product of the velocity and temperature fluctuations at two points $(u_i)_A(\theta\theta)_B$ yields

$$\left(\frac{\partial}{\partial x_k}\right)_A \left(\frac{\partial}{\partial x_k}\right)_B (u_i)_A(\theta\theta)_B = \frac{1}{4}\left(\frac{\partial^2}{\partial x_k \partial x_k}\right)_{AB} (u_i)_A(\theta\theta)_B - \frac{\partial^2}{\partial \xi_k \partial \xi_k}(u_i)_A(\theta\theta)_B. \tag{3.12}$$

Since $(u_i)_A$ can be treated as constant with respect to a derivative at point B and $(\theta\theta)_B$ as constant with respect to a derivative at point A, it follows from (3.12) after averaging

$$\overline{\left(\frac{\partial u_i}{\partial x_k}\right)_A \left(\frac{\partial \theta\theta}{\partial x_k}\right)_B} = \frac{1}{4}\left(\frac{\partial^2}{\partial x_k \partial x_k}\right)_{AB} \overline{(u_i)_A(\theta\theta)_B} - \frac{\partial^2}{\partial \xi_k \partial \xi_k}\overline{(u_i)_A(\theta\theta)_B}. \tag{3.13}$$

Taking the limit for $A \to B$ yields

$$\overline{\frac{\partial u_i}{\partial x_k}\frac{\partial \theta^2}{\partial x_k}} = \tfrac{1}{4}\Delta_x \overline{u_i\theta^2} - \tfrac{1}{2}\left[(\Delta_\xi \overline{u_i\theta'\theta'})_0 + (\Delta_\xi \overline{u_i'\theta\theta})_0\right], \tag{3.14}$$

where $\Delta_x = \partial^2/\partial x_i \partial x_i$ is the Laplace operator with respect to x; prime $'$ indicates the value of the two-point correlation function at the point B, and subscript zero represents the zero separation $\xi = 0$ between two points. For high Reynolds and Péclet numbers, we may expect that turbulence becomes locally quasi-homogeneous. The condition of invariance under translation for a homogeneous flow field yields (see Hinze 1975, chap. 4-3)

$$\overline{u_i\theta'\theta'} = -\overline{u_i'\theta\theta}. \tag{3.15}$$

Differentiation of (3.15) with respect to ξ, and taking $A \to B$ yields

$$(\Delta_\xi \overline{u_i\theta'\theta'})_0 + (\Delta_\xi \overline{u_i'\theta\theta})_0 \to 0, \tag{3.16}$$

if the fine-scale structure of the flow field is locally homogeneous. Thus, for a homogeneous flow field it follows from (3.16) and (3.14), that the right-hand side of (3.14) may reduce to $\Delta_x \overline{u_i\theta^2}/4$, but it is also expected that $\overline{u_i\theta^2}$ becomes negligibly small. We consider the flow field as inhomogeneous so that

$$(\Delta_\xi \overline{u_i\theta'\theta'})_0 + (\Delta_\xi \overline{u_i'\theta\theta})_0 \neq 0.$$

For small separation between the points A and B, we assume the following approximation

$$(\Delta_\xi \overline{u_i\theta'\theta'})_0 \simeq \Delta_x \overline{u_i\theta^2}, \qquad (\Delta_\xi \overline{u_i'\theta\theta})_0 \simeq \Delta_x \overline{u_i\theta^2}. \tag{3.17}$$

From this follows

$$[(\Delta_\xi \overline{u_i\theta'\theta'})_0 + (\Delta_\xi \overline{u_i'\theta\theta})_0] = C\Delta_x \overline{u_i\theta^2} + R, \tag{3.18}$$

where the term R is defined as

$$R \equiv [(\Delta_\xi \overline{u_i\theta'\theta'})_0 + (\Delta_\xi \overline{u_i'\theta\theta})_0] - C\Delta_x \overline{u_i\theta^2},$$

$C \in \mathbb{R}$. From this follows, together with (3.14),

$$R = \left[(\Delta_\xi \overline{u_i \theta' \theta'})_0 + (\Delta_\xi \overline{u_i' \theta\theta})_0\right] - C \Delta_x \overline{u_i \theta^2} \simeq C' \overline{\frac{\partial u_i}{\partial x_k} \frac{\partial \theta^2}{\partial x_k}}, \tag{3.19}$$

$C' \in \mathbb{R}$. For strongly inhomogeneous regions, for example in the near-wall region, we may expect a large absolute value of the left-hand side of (3.18). However, we cannot determine the sign of the left-hand side of (3.18) or of R at this point. From (3.14) and (3.18), we obtain

$$\overline{\frac{\partial u_i}{\partial x_k} \frac{\partial \theta^2}{\partial x_k}} = C_{T1}(\Delta_x \overline{u_i \theta^2} + R), \tag{3.20}$$

$C_{T1} \in \mathbb{R}$. We now make the second assumption. Similarly to Shikazono & Kasagi (1996) and Wörner, Ye & Grötzbach (1999), we assume the following functional relationship between dimensionless quantities

$$\frac{\overline{\frac{\partial u_i}{\partial x_k} \frac{\partial \theta^2}{\partial x_k}}}{\sqrt{\overline{\left(\frac{\partial u_{(i)}}{\partial x_k}\right)^2}} \sqrt{\overline{\left(\frac{\partial \theta}{\partial x_k}\right)^2}} \sqrt{\overline{\theta^2}}} \simeq C_{T2} \frac{\overline{u_i \theta^2}}{\sqrt{\overline{u_{(i)}^2}}\, \overline{\theta^2}}, \tag{3.21}$$

where the indices in parentheses do not obey the summation convention rule. The temperature variance dissipation rate is defined as follows

$$\epsilon_\theta = 2\kappa \overline{\frac{\partial \theta}{\partial x_k} \frac{\partial \theta}{\partial x_k}} = 2\kappa \overline{\left(\frac{\partial \theta}{\partial x_k}\right)^2}, \tag{3.22}$$

and we approximate the ratio of kinetic energy to dissipation rate of velocity component i with the ratio of the total kinetic energy to total dissipation rate

$$\frac{\overline{u_{(i)}^2}}{\overline{\left(\frac{\partial u_{(i)}}{\partial x_k}\right)^2}} \simeq \frac{2k}{\overline{\epsilon}}. \tag{3.23}$$

Using (3.22) and (3.23), we can write (3.21) as

$$\overline{\frac{\partial u_i}{\partial x_k} \frac{\partial \theta^2}{\partial x_k}} = C_{T3} \frac{1}{\sqrt{4\nu\kappa}} \sqrt{\frac{\epsilon}{k} \frac{\epsilon_\theta}{\overline{\theta^2}}} \overline{u_i \theta^2}. \tag{3.24}$$

Being consistent with usual gradient diffusion models, all standard triple correlation models take a negative sign (equations (3.2), (3.3) and (3.5)). This redefines the coefficient to be the negative value of the C_{T3} in (3.24). From this and together with (3.20) and (3.24) we obtain

$$\overline{u_i \theta^2} = -C_\theta 2\sqrt{\nu\kappa} \sqrt{\frac{k}{\epsilon} \frac{\overline{\theta^2}}{\epsilon_\theta}} \left[\Delta_x \overline{u_i \theta^2} + R\right]. \tag{3.25}$$

From (3.19) and (3.24), it follows that $2\sqrt{\nu\kappa}\sqrt{(k/\epsilon)(\overline{\theta^2}/\epsilon_\theta)}\cdot R$ may be approximated with one of the standard models for $\overline{u_i\theta^2}$ resulting in

$$\overline{u_i\theta^2} = -C_\theta\left[2\sqrt{\nu\kappa}\sqrt{\frac{k}{\epsilon}\frac{\overline{\theta^2}}{\epsilon_\theta}}\Delta_x\overline{u_i\theta^2} + \frac{k}{\epsilon}\overline{u_iu_j}\frac{\partial\overline{\theta^2}}{\partial x_j}\right], \tag{3.26}$$

or

$$\overline{u_i\theta^2} = -C_\theta\left[2\sqrt{\nu\kappa}\sqrt{\frac{k}{\epsilon}\frac{\overline{\theta^2}}{\epsilon_\theta}}\Delta_x\overline{u_i\theta^2} + \frac{k^2}{\epsilon}\frac{\partial\overline{\theta^2}}{\partial x_i}\right]. \tag{3.27}$$

The formal derivation of the coefficient $\sqrt{(k/\epsilon)(\overline{\theta^2}/\epsilon_\theta)}$ from (3.25) supports the application of the mixed time scale in the model (3.26)

$$\overline{u_i\theta^2} = -C_\theta\sqrt{\frac{k}{\epsilon}\frac{\overline{\theta^2}}{\epsilon_\theta}}\left[2\sqrt{\nu\kappa}\Delta_x\overline{u_i\theta^2} + \overline{u_iu_j}\frac{\partial\overline{\theta^2}}{\partial x_j}\right], \tag{3.28}$$

or in the model (3.2) resulting in

$$\overline{u_i\theta^2} = -C'_{H\theta}\sqrt{\frac{k}{\epsilon}\frac{\overline{\theta^2}}{\epsilon_\theta}}\overline{u_iu_j}\frac{\partial\overline{\theta^2}}{\partial x_j}. \tag{3.29}$$

The coefficient $C_\theta = 0.11$ is used in the models (3.26), (3.27) and (3.28). In the model (3.29), $C'_{H\theta} = 0.29$ is found to give good predictions for $Pr = 0.71$. Elghobashi & Launder (1983) compared the experimental results of LaRue & Libby (1981) for the thermal mixing layer downstream of a half-heated grid with predictions by model (3.29) and found good agreement using the coefficient $C'_{H\theta} = 0.25$. Similarly, a mixed time scale may be applied in model (3.5) resulting in

$$\overline{u_i\theta^2} = -C_{HL}\sqrt{\frac{k}{\epsilon}\frac{\overline{\theta^2}}{\epsilon_\theta}}\left(\overline{u_iu_j}\frac{\partial\overline{\theta^2}}{\partial x_j} + 2\overline{u_i\theta}\frac{\partial\overline{u_i\theta}}{\partial x_j}\right). \tag{3.30}$$

Approximating the term R in (3.25) with $2\sqrt{\nu\kappa}\sqrt{(k/\epsilon)(\overline{\theta^2}/\epsilon_\theta)}\Delta_x\overline{u_i\theta^2}$ we obtain

$$\overline{u_i\theta^2} = -C_{D\theta}2\sqrt{\nu\kappa}\sqrt{\frac{k}{\epsilon}\frac{\overline{\theta^2}}{\epsilon_\theta}}\Delta_x\overline{u_i\theta^2}, \tag{3.31}$$

with the new coefficient $C_{D\theta}$. For comparison, we will use $C_{D\theta} = 0.22$.

A numerically and physically simpler model, which can cover a wide range of Prandtl numbers, may be given as

$$\overline{u_i\theta^2} = -C_{D\theta}\sqrt{Pr}\frac{k}{\epsilon}\overline{u_iu_j}\frac{\partial\overline{\theta^2}}{\partial x_j}, \tag{3.32}$$

where the same coefficient, $C_{D\theta} = 0.22$, as used in the models (3.2) and (3.31) is taken for comparison.

Figure 9*a* shows vertical profiles of $D^t_\theta = (\partial/\partial x_i)\overline{u_i\theta^2}$ as evaluated from DNS, and DNS based results for D^t_θ as predicted by the models (3.2), (3.3), (3.4), (3.6) and (3.32) for $Pr = 0.025$. As indicated in figure 6*a* standard models (3.2), (3.3) and the model (3.6) strongly overpredict the DNS results. Models (3.2) and (3.6) give the correct position

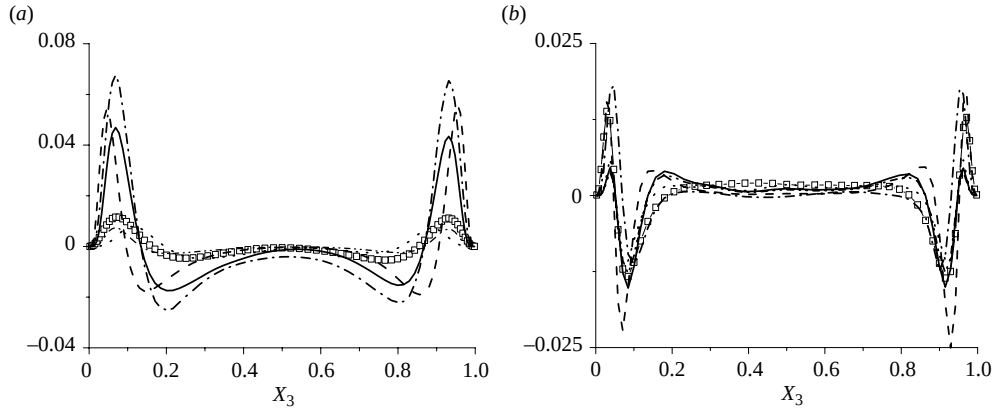

FIGURE 9. □, Evaluated vertical profile of D_θ^t for (*a*) $Pr = 0.025$, (*b*) 0.71. DNS based results for D_θ^t as predicted by the equations (3.2) —, (3.3) – – –, (3.4) · · ·, (3.6) – · – and (3.32) - · · -, for (*a*) $Pr = 0.025$, (*b*) 0.71.

where the model (3.3) slightly misplaces the maximum point. Replacing the mechanical time scale with the thermal time scale as done in model (3.4) will underpredict the maximum point and give qualitatively different results within the thermal boundary layer at this Rayleigh number, as already indicated in the previous section (see figure 7). Model (3.32) gives better results, but underpredicts the maxima considerably.

For $Pr = 0.71$, a similar comparison is given in figure 9*b*. Results due to model (3.2) show overpredictions at the edge of the thermal boundary layer and strong underprediction in the near-wall region. Taking the thermal time scale in the diffusion model, equation (3.4), gives good prediction of the minimum point and improves the results at the edge of the boundary layer, but yields even stronger underprediction in the near-wall region compared to the results of model (3.2). Model (3.3) considerably overpredicts the minimum point and the results at the edge of the boundary layer. Fortunately, model (3.3) gives good prediction of the maximum point. Model (3.6) performs well at the edge of the boundary layer and gives small overprediction within the boundary layer and of the maximum point while underpredicting the minima. Model (3.32) gives very similar results to model (3.2).

For the case $Pr = 0.71$, we conclude that the coefficients of the standard models are well optimized. However, considering results for the case of $Pr = 0.025$, we find overpredictions of the maxima up to seven times, as in the results given by model (3.6), while using the same coefficients. Application of the thermal, instead of mechanical, time scale in the standard model for D_θ^t results in qualitatively wrong predictions within the thermal boundary layer for $Pr = 0.025$ and $Ra = 1 \times 10^5$. A minimum level of improvement for standard models will be the introduction of the Prandtl number in the empirical coefficient, as done in model (3.32). Model (3.32) performs similarly to model (3.2) in the case $Pr = 0.71$, and gives comparably good results in the case $Pr = 0.025$, but underpredicts the maxima by about 40% in the case $Pr = 0.025$.

Figure 10 shows the vertical profiles of D_θ^t as evaluated from the DNS, and the DNS based results for D_θ^t as predicted by the models (3.5), (3.26), (3.27), (3.28), (3.29), (3.30) and (3.31), for $Pr = 0.025$ and $Pr = 0.71$ respectively.

First, we compare the predictions given by the models (3.5), (3.29) and (3.30). This comparison allows the analysis of the influence of the mixed time scale on the standard turbulent diffusion models. Predictions by model (3.29) show a big

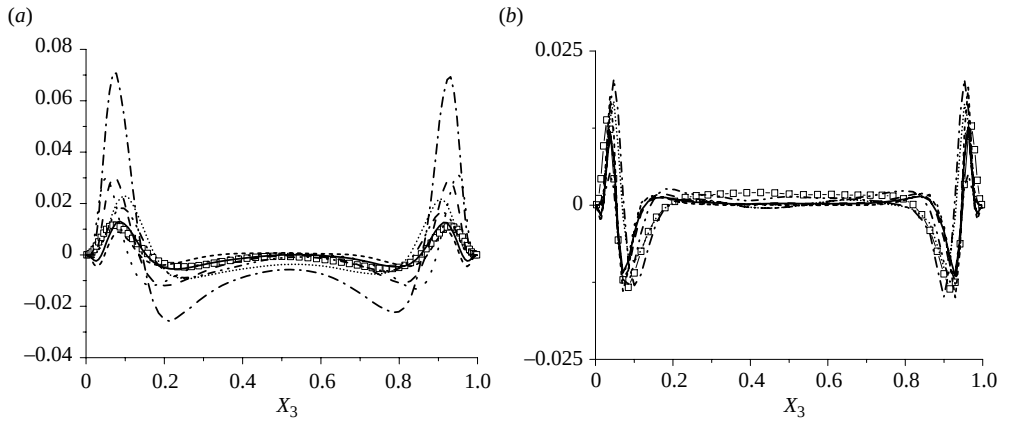

FIGURE 10. □, Evaluated vertical profile of D_θ^t for (*a*) $Pr = 0.025$, (*b*) 0.71. DNS based results for D_θ^t as predicted by the equations (3.5) - · -, (3.26) – – –, (3.27) · · ·, (3.28) —, (3.29) – · · –, (3.30) · · · and (3.31) - - -, for (*a*) $Pr = 0.025$, (*b*) 0.71.

improvement compared to the standard gradient diffusion model (equation (3.2)) in the case $Pr = 0.025$, since the model given by equation (3.2) overpredicts the case $Pr = 0.025$ by about four times. However, the major deficiency of the simple gradient diffusion model (equation (3.2)) cannot be recovered if the mixed time scale is used; then the model still underestimates the maxima by about three times in the case $Pr = 0.71$ while it overpredicts the maxima by about 50% in the case $Pr = 0.025$. Model (3.5) considers the mechanical time scale and gives fairly good predictions for $Pr = 0.71$, but strongly overpredicts the case $Pr = 0.025$ since the added production term cannot account for the large thermal diffusivity of the low-Prandtl-number fluids. Taking now the mixed time scale for the same model (equation (3.30)) gives very good predictions at the edge of the thermal boundary layer, but yields values that are too low for the minimum point for $Pr = 0.71$. Considering the mixed time scale yields a big improvement of the model in the case $Pr = 0.025$, as shown in figure 10(*a*). However, assuming the mixed time scale does not improve the deficiencies of the models within the thermal boundary layer, and, although improving the case $Pr = 0.025$ strongly, still yields a large overprediction of the maxima (by about 100% by the equation (3.30)).

We discuss now the results of models (3.26), (3.27) and (3.28) together, since these models are simple variations of equation (3.25), and compare them with results of model (3.31). Since model (3.26) is formally similar to model (3.5), the coefficient C_θ is intentionally fixed to the value $C_\theta = 0.11$ for models (3.26), (3.27) and (3.28), which is the suggested value for triple correlation models by Hanjalić & Launder (1976) and Dol *et al.* (1997). This allows us to compare the new models with the standard model (equation (3.5)). In the model (3.31), the term R is also approximated with $2\sqrt{\nu\kappa}\sqrt{(k/\epsilon)(\overline{\theta^2}/\epsilon_\theta)\Delta_x \overline{u_i\theta^2}}$, so that a value of the coefficient will be considered as the double of the value of the coefficient used in (3.26), and therefore $C_{D\theta} = 0.22$. Notice that 0.22 is also the suggested coefficient value for the standard gradient diffusion model (3.2). Fixing the coefficients in this way enables a first analysis of the description of R, and of the influence of the time scale on the performance of the basic model, equation (3.25).

Figure 10(*b*) shows good predictions of the maxima and minima by models (3.26), (3.27), (3.28) and (3.31) for the case $Pr = 0.71$. These results show very good predictions

within the thermal boundary layer and some improvement of the standard model (equations (3.2) and (3.3)) at the edge of the boundary layer. However, the results still give an underprediction at the edge of the boundary layer. For the case $Pr = 0.71$, the coefficient in equations (3.26), (3.27), (3.28) and (3.31) seems to require only a minimal optimization depending on the description of R and of the choice of the time scale.

For the case $Pr = 0.025$, a similar comparison is shown in figure 10(a). Model (3.26) differs from the standard model (3.5) only in one term so that a direct comparison may indicate the influence of the new formulation. Model (3.26) shows quantitatively much better results as compared with the predictions by model (3.5), but still produces values of the maxima that are too large. Model (3.27) performs similarly to model (3.26), resulting in much better, but still too large, predictions of the maxima. In model (3.27), the term R is approximated by equation (3.3). Owing to this description of R, model (3.27) yields, similarly to model (3.3), a slightly misplaced position of the maxima (figures 10a and 9a). For the case when a mixed time scale is used, a direct comparison of models (3.28) and (3.30) shows a similar improvement of the new model formulation. Model (3.28) gives very good predictions in the channel centre and within the thermal boundary layer, but slightly underpredicts in the near-wall region. Results given by model (3.30) overpredict the maximum point by about 100% (figure 10a). Model (3.31) gives a good approximation of D_θ^t in the channel centre and within the thermal boundary layer, but underestimates the near wall region.

These results indicate that, for $Pr \sim 1$, an application of the mixed time scale in model (3.5), as given by model (3.30), will give a good approximation of D_θ^t. However, in the case $Pr = 0.025$, this approximation does not give satisfactory results since model (3.30) overpredicts the maxima by about 100%. This deficiency may be resolved if the approach introduced in this section is applied, then model (3.28) gives good predictions for both cases ($Pr = 0.025$ and $Pr = 0.71$), while the same empirical coefficient is used (figures 10(a) and 10(b)).

3.2.3. *Discussion of the new model for the turbulent diffusion* D_θ^t

Model (3.28) introduces the term $2\sqrt{\nu\kappa}\sqrt{(k/\epsilon)(\overline{\theta^2}/\epsilon_\theta)}\Delta_x\overline{u_i\theta^2}$ to approximate the vector $\overline{u_i\theta^2}$. In the following, we discuss this term in more detail. Normalization introduced in the § 2 yields

$$2\sqrt{\nu\kappa} = \frac{2}{Re_0 Pr^{1/2}}.$$

For high Reynolds numbers, we may expect that the transport due to the turbulent diffusion becomes negligibly small compared to the other terms, so that the production and the dissipation rate are in local equilibrium. The coefficient $C_\theta(2/Re_0Pr^{1/2})\sqrt{(k/\epsilon)(\overline{\theta^2}/\epsilon_\theta)}$ used in models (3.26), (3.27), (3.28) and (3.31) is consistent with this argumentation.

$Re_0 \ll 1$ may give a large value of the coefficient $C_\theta(2/Re_0Pr^{1/2})\sqrt{(k/\epsilon)(\overline{\theta^2}/\epsilon_\theta)}$ and therefore can result in numerical instability. However, beyond some critical Reynolds number, the term $\sqrt{(k/\epsilon)(\overline{\theta^2}/\epsilon_\theta)}$ vanishes. A slight numerical disadvantage of the model is induced by the term $\Delta_x\overline{u_i\theta^2}$ since second derivatives necessitate finer grids. Accuracy and numerical stability of the solution strongly depend on the value of the coefficient $C_\theta(2/Re_0Pr^{1/2})\sqrt{(k/\epsilon)(\overline{\theta^2}/\epsilon_\theta)}$. In fact, equation (3.25), and variations of this equation given by (3.26), (3.27) and (3.28), represent a Helmholtz equation

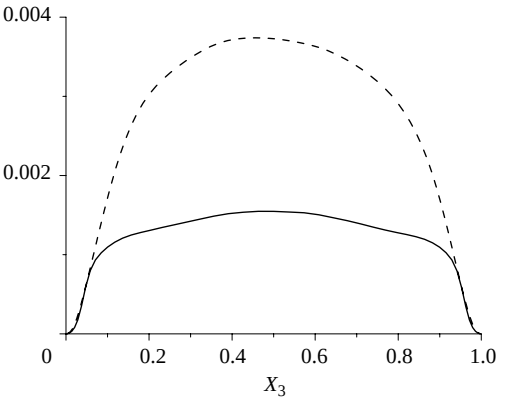

FIGURE 11. DNS-evaluated vertical profiles of the coefficient $C_\theta(2/Re_0Pr^{1/2})\sqrt{(k/\epsilon)(\overline{\theta^2}/\epsilon_\theta)}$ for $Pr = 0.025$ – – –, and for $Pr = 0.71$ —.

with a real coefficient $C_\theta(2/Re_0Pr^{1/2})\sqrt{(k/\epsilon)(\overline{\theta^2}/\epsilon_\theta)}$. Equation (3.31) is a homogeneous Helmholtz equation. It is well known that the accuracy of the numerical solution to the Helmholtz equation depends significantly on the physical coefficient (here $C_\theta(2/Re_0Pr^{1/2})\sqrt{(k/\epsilon)(\overline{\theta^2}/\epsilon_\theta)}$) and that the mesh-width should be adjusted on this coefficient (see e.g. Ihlenburg & Babuška 1995). Bayliss, Goldstein & Turkel (1985) show that the quality of the numerical results deteriorates as the coefficient in the Helmholtz equation increases and state a convergence theorem under the assumption that coefficient × mesh width is sufficiently small. In practice, we usually follow a simple rule

$$coefficient \times mesh\ width = const.$$

(Harari & Hughes 1991). In computations with low coefficients, this rule leads to sufficiently good results. Figure 11 shows vertical profiles of the coefficient $C_\theta(2/Re_0Pr^{1/2})\sqrt{(k/\epsilon)(\overline{\theta^2}/\epsilon_\theta)}$ as evaluated from the DNS for the cases $Pr = 0.025$ and $Pr = 0.71$. We recall that in the normalization used here, $Re_0 = 941.9$ and $Re_0 = 2000$ for the cases $Pr = 0.71$ and $Pr = 0.025$, respectively. Figure 11 shows very low values of the coefficient for the cases considered, and indicates that convergence problems in the numerical solution of model (3.28) may occur only at very low Reynolds and Prandtl numbers. However, the term $\sqrt{(k/\epsilon)(\overline{\theta^2}/\epsilon_\theta)}$ in the coefficient vanishes beyond some critical Reynolds number, as pointed out above. The new modelling approach introduced in this section results in a Helmholtz equation and represents a simple linear approximation of the nonlinear transport equation for $\overline{u_i\theta^2}$. The coefficient for the Laplacian considers mixed time scales $(k/\epsilon)(\overline{\theta^2}/\epsilon_\theta)$. Because the model should approximate $\overline{u_i\theta^2}$ in the entire flow field and at all scales an application of the mixed time scales in the coefficient is physically consistent.

This modelling approach yields also a good approximation of the turbulent diffusion in the temperature variance dissipation rate equation where standard models show strong deficiencies or fail completely. However, the generality and performance of the models based on the new modelling approach can only be proved when they are successfully applied to different types of flow.

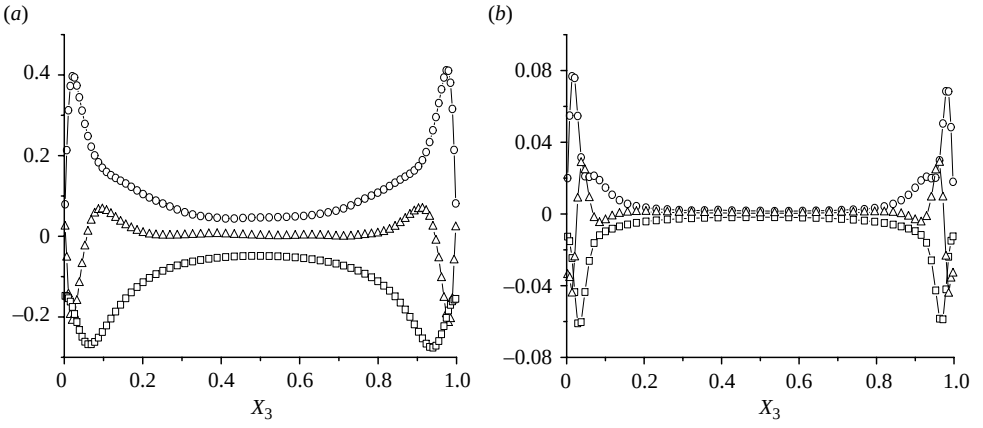

FIGURE 12. Vertical profiles of ○, P_Σ; △, D_{ϵ_θ}; and □, D in equation (4.1), for (*a*) $Pr = 0.025$, (*b*) 0.71.

4. Temperature variance dissipation rate

In the following, we discuss the temperature variance dissipation rate ϵ_θ which is the second term that must be modelled in order to close the transport equation for the temperature variance (equation (3.1)). ϵ_θ is often modelled assuming a constant value of the thermal to mechanical time scale ratio $\mathscr{R} = (\overline{\theta^2}/\epsilon_\theta)(\epsilon/k)$. However, figure 8 shows that this assumption necessarily leads to wrong predictions for the cases $Pr = 0.025$, $Ra = 10^5$, and $Pr = 0.71$, $Ra = 6.3 \times 10^5$ and indicates that a modelled transport equation for the temperature variance dissipation rate may give better predictions and that it may cover a wide range of Prandtl and Rayleigh numbers.

4.1. *Analysis of the transport equation for the temperature variance dissipation rate*

The transport equation for the dissipation rate ϵ_θ of the temperature variance $\overline{\theta^2}$ can be derived from the energy equation:

$$\frac{\partial \epsilon_\theta}{\partial t} + \overline{U_i}\frac{\partial \epsilon_\theta}{\partial x_i} = \underbrace{\underbrace{-\frac{\partial}{\partial x_i}\overline{u_i \epsilon_\theta^*}}_{D^t_{\epsilon_\theta}} + \underbrace{\kappa \frac{\partial^2 \epsilon_\theta}{\partial x_i \partial x_i}}_{D^m_{\epsilon_\theta}}}_{D_{\epsilon_\theta}}$$
$$\underbrace{-2\kappa \overline{\frac{\partial u_i}{\partial x_j}\frac{\partial \theta}{\partial x_j}\frac{\partial T}{\partial x_i}}}_{P_I} \underbrace{-2\kappa \overline{\frac{\partial \theta}{\partial x_i}\frac{\partial \theta}{\partial x_j}\frac{\partial \overline{U_i}}{\partial x_j}}}_{P_{II}} \underbrace{-2\kappa u_i \overline{\frac{\partial \theta}{\partial x_j}\frac{\partial^2 T}{\partial x_i \partial x_j}}}_{P_{III}}$$
$$\underbrace{-2\kappa \overline{\frac{\partial u_i}{\partial x_j}\frac{\partial \theta}{\partial x_j}\frac{\partial \theta}{\partial x_i}}}_{P_{IV}} \underbrace{-2\kappa^2 \overline{\frac{\partial^2 \theta}{\partial x_i \partial x_j}\frac{\partial^2 \theta}{\partial x_i \partial x_j}}}_{D}, \tag{4.1}$$

where $\epsilon_\theta^* = \kappa(\partial\theta/\partial x_k)(\partial\theta/\partial x_k)$ and $\overline{\epsilon_\theta^*} = \epsilon_\theta$. From the DNS data for the Rayleigh–Bénard convection at $Pr = 0.025$ and $Pr = 0.71$, each term of (4.1) is calculated.

Figure 12 shows evaluated budgets of ϵ_θ at $Pr = 0.025$ and $Pr = 0.71$ where the production terms are summed up $P_\Sigma = P_I + P_{II} + P_{III} + P_{IV}$. Outside the thermal boundary layers, the diffusive transport is positive but very small for both Prandtl numbers. Thus, the production and destruction terms are almost in local equilibrium.

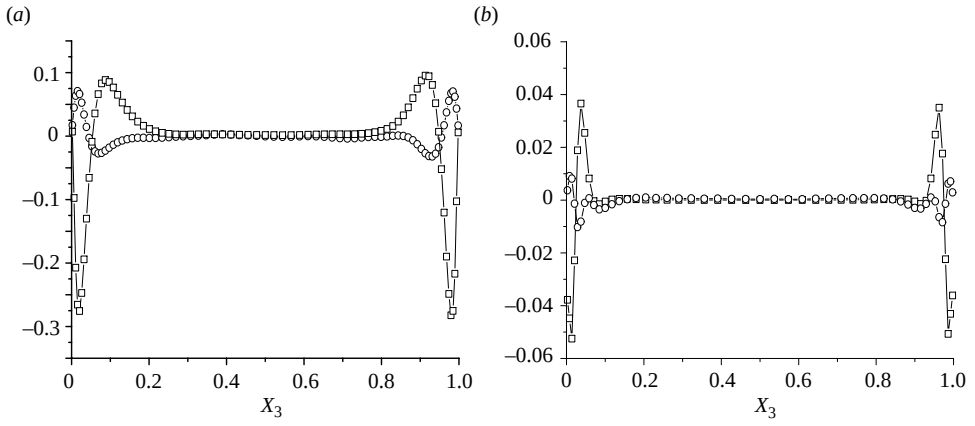

FIGURE 13. Vertical profiles of □, $D^m_{\epsilon_\theta}$ and ○, $D^t_{\epsilon_\theta}$ for (*a*) $Pr = 0.025$, (*b*) 0.71.

Inside the boundary layers, the term P_Σ and the destruction term D show peaks at different wall distances. In these regions, the diffusive transport D_{ϵ_θ} is very important, since it balances this difference by redistributing ϵ_θ from the near-wall region to the channel centre.

Figure 13 shows the contribution of the molecular $D^m_{\epsilon_\theta}$ and turbulent diffusion term $D^t_{\epsilon_\theta}$ to the total diffusion D_{ϵ_θ} in the cases considered. Near the walls, $D^m_{\epsilon_\theta}$ is one of the dominant terms in the budget of ϵ_θ. Similar results from DNS data for $Pr = 0.006$ and $Ra = 24\,000$ are obtained by Wörner & Grötzbach (1996*a*).

4.2. *Analysis of existing and development of a new model for the turbulent diffusion* $D^t_{\epsilon_\theta}$

The correlation $\overline{u_i \epsilon^*_\theta}$ is often modelled using the gradient hypothesis (see e.g. Nagano & Kim 1988)

$$\overline{u_i \epsilon^*_\theta} = -C_{D\epsilon_\theta} \frac{k}{\epsilon} \overline{u_i u_j} \frac{\partial \epsilon_\theta}{\partial x_j}, \tag{4.2}$$

or when replacing the tensor $(k/\epsilon)\overline{u_i u_j}$ by the scalar form k^2/ϵ as

$$\overline{u_i \epsilon^*_\theta} = -C_{S\epsilon_\theta} \frac{k^2}{\epsilon} \frac{\partial \epsilon_\theta}{\partial x_i}. \tag{4.3}$$

As introduced in § 3.1, the points A and B of the relative coordinate system are arbitrary, so it follows that:

$$\begin{aligned} (\Delta_\xi \overline{\theta u_i' \theta'})_0 &= (\Delta_\xi \overline{\theta' u_i \theta})_0, \\ (\Delta_\xi \overline{\theta \theta u_i'})_0 &= (\Delta_\xi \overline{\theta' \theta' u_i})_0. \end{aligned} \tag{4.4}$$

Using the differential operator (3.11) and equations (4.4), the transport term $\overline{u_i \epsilon^*_\theta}$ can be written as

$$\overline{u_i \epsilon^*_\theta} = \kappa \tfrac{1}{8} \Delta_x \overline{u_i \theta^2} - \kappa [(\Delta_\xi \overline{u_i \theta \theta'})_0 + \tfrac{1}{2} (\Delta_\xi \overline{u_i' \theta \theta})_0]. \tag{4.5}$$

If the fine-scale structure of the turbulence field is locally homogeneous, it follows

that (see Hinze 1975, chap. 4-3):

$$(\Delta_\xi \overline{u_i\theta\theta'})_0 \simeq -(\Delta_\xi \overline{u_i'\theta'\theta})_0,$$
$$(\Delta_\xi \overline{u_i'\theta\theta})_0 \simeq -(\Delta_\xi \overline{u_i\theta'\theta'})_0, \tag{4.6}$$

and with (4.4) this yields

$$(\Delta_\xi \overline{u_i\theta\theta'})_0 \simeq (\Delta_\xi \overline{u_i'\theta\theta})_0 \simeq 0. \tag{4.7}$$

The correlation $\overline{u_i\epsilon_\theta^*}$ describes the transport from the walls to the channel centre. This transport is locally strongly inhomogeneous at low and moderate Reynolds and Péclet numbers. We consider the flow field as inhomogeneous so that

$$(\Delta_\xi \overline{u_i\theta\theta'})_0 \neq 0, \quad (\Delta_\xi \overline{u_i'\theta\theta})_0 \neq 0,$$

and for a small separation between the points A and B, we assume the following approximation

$$(\Delta_\xi \overline{u_i\theta\theta'})_0 \simeq \Delta_x \overline{u_i\theta^2}, \qquad (\Delta_\xi \overline{u_i'\theta\theta})_0 \simeq \Delta_x \overline{u_i\theta^2}. \tag{4.8}$$

Therefore, analogously to the derivation introduced in the previous section, we write (4.5) for small separation between points A and B as

$$\overline{u_i\epsilon_\theta^*} = -C_{DT}(\kappa \Delta_x \overline{u_i\theta^2} + R_\epsilon), \tag{4.9}$$

where the term $R_\epsilon \simeq C'\overline{u_i\epsilon_\theta^*}$ for some $C' \in \mathbb{R}$. However, we cannot determine the sign of R_ϵ at this point. R_ϵ can be described by the term $\kappa \Delta_x \overline{u_i\theta^2}$ resulting in

$$\overline{u_i\epsilon_\theta^*} = -C_{DT}^* \, \kappa \Delta_x \overline{u_i\theta^2}, \tag{4.10}$$

or using a standard model for $\overline{u_i\epsilon_\theta^*}$.
From (3.31) we obtain

$$-\kappa \Delta_x \overline{u_i\theta^2} = C^* \sqrt{\frac{1}{Pr}\frac{\epsilon}{k}\frac{\epsilon_\theta}{\theta^2}} \, \overline{u_i\theta^2}. \tag{4.11}$$

Equations (4.10) and (4.11) yield the simple model

$$\overline{u_i\epsilon_\theta^*} = C_{DT}^T \sqrt{\frac{1}{Pr}\frac{\epsilon}{k}\frac{\epsilon_\theta}{\theta^2}} \, \overline{u_i\theta^2}. \tag{4.12}$$

Equations (4.9) and (4.11) yield

$$\overline{u_i\epsilon_\theta^*} = C_{DT}^T \sqrt{\frac{1}{Pr}\frac{\epsilon}{k}\frac{\epsilon_\theta}{\theta^2}} \, \overline{u_i\theta^2} - C_{DT} R_\epsilon. \tag{4.13}$$

Figure 14 shows vertical profiles of the $\overline{u_i\epsilon_\theta^*}$ for Rayleigh–Bénard convection evaluated from the DNS data at Prandtl numbers $Pr = 0.025$ and $Pr = 0.71$. The net contribution of $\overline{u_i\epsilon_\theta^*}$ to ϵ_θ is zero, since it acts as a redistribution term. Apart of the thermal boundary layer, this transport shows almost linear profiles for both cases considered. Within the thermal boundary layer, the term $\overline{u_i\epsilon_\theta^*}$ shows one local extremum for the case $Pr = 0.025$, $Ra = 100\,000$. For $Pr = 0.71$, $Ra = 630\,000$, DNS results show local minima, maxima and an additional change of a gradient within the thermal boundary layer. Figure 15 contains vertical profiles of $\overline{u_i\epsilon_\theta^*}$ as calculated by equations (4.2), (4.3) and (4.12) using DNS data, where the standard coefficients $C_{D\epsilon_\theta} = 0.22$, $C_{S\epsilon_\theta} = 0.3$ are used in equations (4.2) and (4.3), respectively. The coefficient in (4.12) is simply set as $C_{DT}^T = 1$.

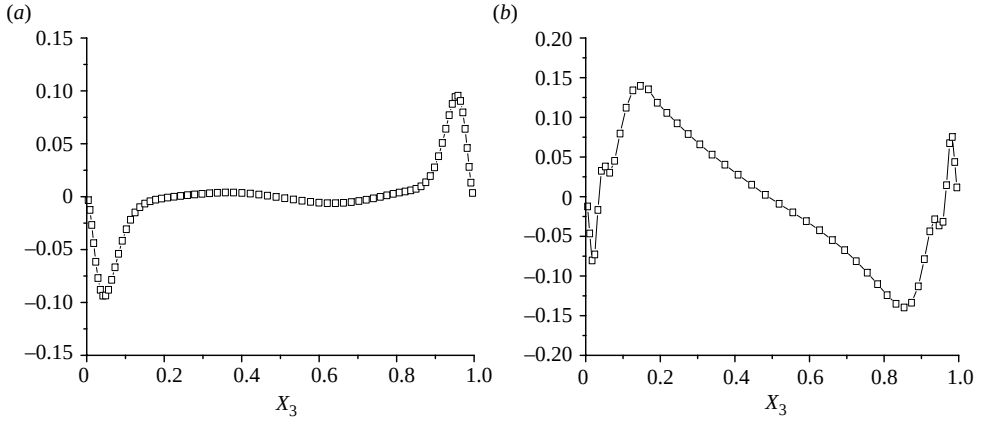

FIGURE 14. □, Evaluated vertical profile of $\overline{u_i \epsilon_\theta^*}$ for (*a*) $Pr = 0.025$, (*b*) 0.71.

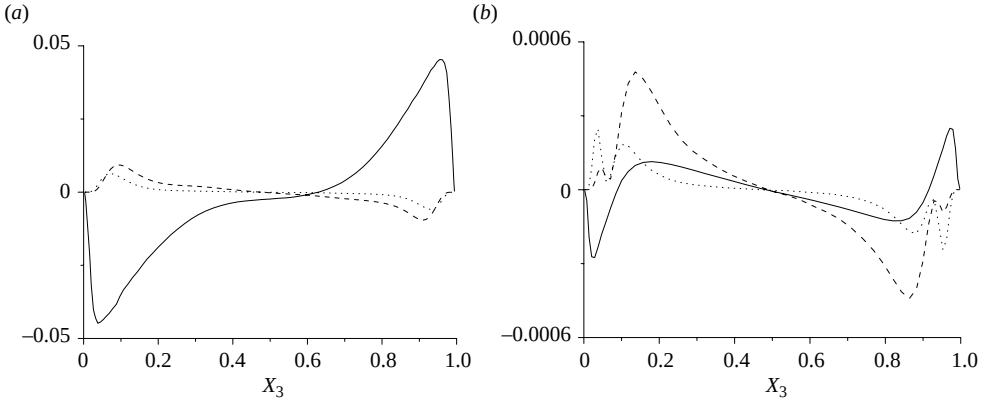

FIGURE 15. Vertical profile of $\overline{u_i \epsilon_\theta^*}$ predicted by (4.12) —, by (4.2) – – – and by (4.3) ···, for (*a*) $Pr = 0.025$, (*b*) 0.71.

We first compare predictions for $Pr = 0.025$ (figure 15*a*) with DNS result (figure 14*a*). Model (4.12) gives qualitatively good predictions, whereas models (4.2) and (4.3) give acceptable predictions in the channel centre, but completely fail within the thermal boundary layer at this Rayleigh number. Quantitatively, model (4.12) is about two times too low.

Comparing predictions for $Pr = 0.71$ (figure 15*b*) with DNS results (figure 14*b*) qualitatively, we see that model (4.12) predicts the near-wall range well, but does not describe the change of gradient in the thermal boundary layer. In contrast to this, models (4.2) and (4.3) predict the change of gradient, but not the change of sign in the near-wall region. In the channel centre, model (4.2) gives qualitatively good predictions whereas models (4.12) and (4.3) have a correct trend and would give qualitatively good predictions for larger coefficients. Quantitatively, all three models are about three orders of magnitude too low at this Rayleigh number.

From these comparisons, it follows that the description of the term R_ϵ in the model (4.13) with a standard model for $\overline{u_i \epsilon_\theta^*}$ (equations (4.2) and (4.3)), and with an additional empirical coefficient may give a better approximation. Equations (4.13),

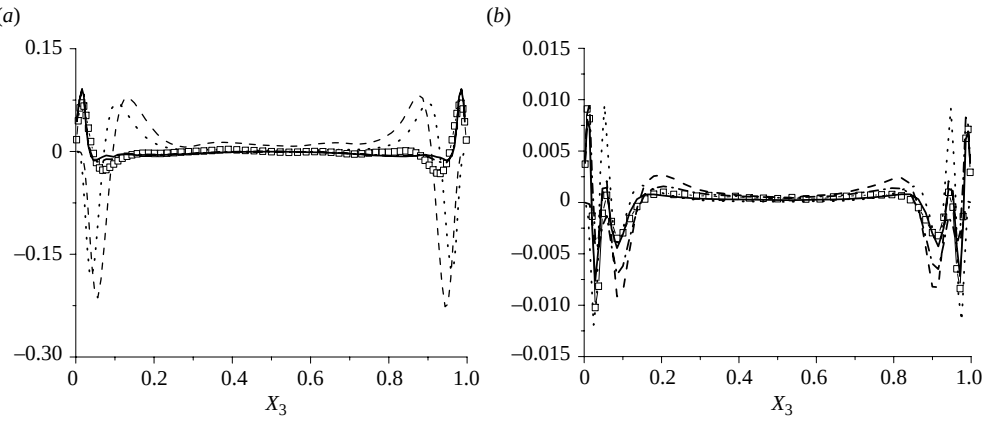

FIGURE 16. □, Evaluated vertical profile of $D^t_{\epsilon_\theta}$ for (*a*) $Pr = 0.025$, (*b*) 0.71. DNS based results for $D^t_{\epsilon_\theta}$ as predicted by the equations (4.2) – – –, (4.3) ···, (4.14) — and (4.15) – · –, for (*a*) $Pr = 0.025$, (*b*) 0.71.

(4.2) and (4.3) with the empirical coefficient $Pr^{0.75}$ yield the following new models

$$\overline{u_i \epsilon^*_\theta} = -Pr^{0.75} C^T_{\epsilon_\theta} \left[\frac{k}{\epsilon} \overline{u_i u_j} \frac{\partial \epsilon_\theta}{\partial x_j} - \sqrt{\frac{1}{Pr} \frac{\epsilon}{k} \frac{\epsilon_\theta}{\theta^2}} \overline{u_i \theta^2} \right], \tag{4.14}$$

and

$$\overline{u_i \epsilon^*_\theta} = -Pr^{0.75} C^T_{\epsilon_\theta} \left[\frac{k^2}{\epsilon} \frac{\partial \epsilon_\theta}{\partial x_j} - \sqrt{\frac{1}{Pr} \frac{\epsilon}{k} \frac{\epsilon_\theta}{\theta^2}} \overline{u_i \theta^2} \right]. \tag{4.15}$$

In order to compare the results, we set the coefficient in models (4.14) and (4.15) to the same value $C^T_{\epsilon_\theta} = 0.7$.

In figure 16(*a*) DNS results, for the turbulent diffusion $D^t_{\epsilon_\theta}$ at $Pr = 0.025$ are compared with the predictions by standard models (4.2) and (4.3) and with the predictions by the new models (4.14) and (4.15). As indicated in figure 15*a*, models (4.2) and (4.3) yield qualitatively wrong results apart from the channel centre at this Rayleigh number. The new models (4.14) and (4.15) predict $D^t_{\epsilon_\theta}$ well, however, both models underpredict the minimum point. Notice that the coefficient for both equations, (4.14) and (4.15), is taken as $C^T_{\epsilon_\theta} = 0.7$.

Figure 16(*b*) shows a similar comparison for $Pr = 0.71$. Standard models still show strong deficiencies within the thermal boundary layer. In the near-wall region, these models do not account for the sign-change, giving qualitatively wrong results at this Rayleigh number. Model (4.15) gives good results in the channel centre and in the near-wall region, but underpredicts the DNS result within the thermal boundary layer. Model (4.14) reproduces the DNS results very well. This analysis shows that model (4.14) may give a good approximation of the turbulent diffusion term $D^t_{\epsilon_\theta}$ for a wide range of low-Prandtl-number flows.

Considering model (4.14) and the model equations for the temperature variance dissipation rate as suggested by Nagano & Kim (1988) and Hanjalić (1994) results in the complete model equation for thetemperature variance dissipation rate ϵ_θ for

Rayleigh–Bénard convection, i.e. without mean velocities,

$$\frac{\partial \epsilon_\theta}{\partial t} = \frac{\partial}{\partial x_i}\left[Pr^{0.75} C_{\epsilon_\theta}^{T} \left[\frac{k}{\epsilon} \overline{u_i u_j} \frac{\partial \epsilon_\theta}{\partial x_i} - \sqrt{\frac{1}{Pr}\frac{\epsilon}{k}\frac{\epsilon_\theta}{\theta^2}} \overline{u_i \theta^2} \right] + \kappa \frac{\partial \epsilon_\theta}{\partial x_i} \right] - C_{P1} \frac{\epsilon_\theta}{\overline{\theta^2}} \overline{u_i \theta} \frac{\partial \overline{T}}{\partial x_i} - C_{D1} \frac{\epsilon_\theta^2}{\overline{\theta^2}}. \quad (4.16)$$

C_{P1}, C_{D1} are functions of the Prandtl number, Rayleigh number and of the turbulent time scale ratio.

5. Conclusions

Based on new direct numerical simulation of turbulent Rayleigh–Bénard convection for the Prandtl number $Pr = 0.025$ and the Rayleigh number $Ra = 10^5$, an analysis of some statistical turbulence quantities has been performed. Some of the characteristics of turbulent convection in low-Prandtl-number flows are shown and discussed. It is found that the modelling of the turbulent heat flux for the Rayleigh–Bénard convection by means of the turbulent Prandtl number concept has serious deficiencies. This analysis indicates that a model of the turbulent heat flux which accounts better for the turbulent convection in low-Prandtl-number fluids should be based on transport equations for the heat fluxes, for the temperature variance, and for the temperature variance dissipation rate, or at least on simplified algebraic forms of these equations.

DNS results are used for the detailed analysis of the transport equation for the temperature variance $\overline{\theta^2}$ and the transport equation for the temperature variance dissipation rate ϵ_θ. This analysis shows the relevance of the turbulent diffusion terms in the near-wall region and in the channel centre as well.

Based on new DNS results and on former DNS results for $Pr = 0.71$, $Ra = 630\,000$, different models for the turbulent diffusion of the temperature variance known from the literature are investigated. This analysis shows that model-coefficients suggested in the literature are well optimized for the case $Pr = 0.71$. However, the analysis shows strong quantitative deficiencies of the models for the case $Pr = 0.025$ since the models overpredict DNS results up to a factor of seven. These results lead to the conclusion that the modelling of the turbulent diffusion term in the temperature variance equation requires the explicit influence of the molecular fluid properties, and that considering only the mechanical or only the thermal time scale is not sufficient for approximation of turbulent diffusion in the temperature variance equation for a wide range of Prandtl numbers. This analysis supports the conclusion that the mixed time scale should be used for modelling of the turbulent diffusion. These results also indicate that for $Pr \sim 1$, an application of the mixed time scale in the Hanjalić–Launder model (equation (3.5)), as given by model (3.30), may give a good approximation of the turbulent diffusion of the temperature variance. In the case $Pr = 0.025$, this approximation does not give satisfactory results since this model (equation (3.30)) overpredicts the maxima by about 100%.

Based on the two-point correlation technique, a novel approach for modelling of the turbulent diffusion of the temperature variance is introduced, which may resolve this deficiency. The new modelling approach results in a Helmholtz equation and represents a linear approximation of the nonlinear transport equation for the turbulent diffusion. This new model (equation (3.28)) considers a mixed time scale and explicitly considers the molecular fluid properties. Major advantages of the new model are very good predictions for both cases ($Pr = 0.025$ and $Pr = 0.71$), and that the same

empirical coefficient is used for both Prandtl numbers. A possible disadvantage of the new model is induced by the Laplace operator in the Helmholtz equation since the second derivatives may necessitate finer grids or overestimate small changes of gradients.

Based on the DNS results for the cases $Pr = 0.025$ and $Pr = 0.71$, standard models for the turbulent diffusion of the temperature variance dissipation rate known from the literature are investigated. This analysis shows that standard models have strong deficiencies or fail qualitatively at the edge and within the thermal boundary layer for the cases considered. The new modelling approach developed for the turbulent diffusion term in the temperature variance equation is analogously applied for modelling of the turbulent diffusion term in the temperature variance dissipation rate equation. Major advantages of the new model (equation (4.14)) are very satisfactory predictions for both cases ($Pr = 0.025$ and $Pr = 0.71$), while the same empirical coefficient is used for both Prandtl numbers. An additional advantage is a minimal increase in model complexity which makes no special demands on model implementation into computer codes.

However, the true generality of the models based on the new modelling approach can only be proved when they are successfully applied to different types of problems, for example to flows in more complex domains.

This research received financial support (GR 1901) from the Deutsche Forschungsgemeinschaft (DFG). The authors gratefully acknowledge this support.

REFERENCES

Bayliss, A., Goldstein, C. & Turkel, E. 1985 On accuracy conditions for the numerical computations of waves. *J. Comput. Phys* **59**, 396–404.

Boudjemadi, R., Maupu, V., Laurence, D. & Le Quéré, P. 1996 Direct numerical simulation of natural convection in a vertical channel: a tool for second moment closure modeling. In *Engineering Turbulence Modelling and Experiments 3* (ed. W. Rodi & G. Bergels), pp. 39–48. Elsevier.

Bunk, M. & Wörner, M. 1998 Direkte numerische Simulation turbulenter Rayleigh–Bénard-Konvektion in Quecksilber. *Tech. Rep.* FZKA 5915. Forschungszentrum Karlsruhe.

Burgers, J. 1953 Some consideration on turbulent flow with shear. In *Proc. K. Ned. Akad. Wet. Ser. B*, Vol. 6, pp. 125–147.

Chou, P. 1945 On the velocity correlation and the solution of the equation of turbulent fluctuations. *Q. Appl. Maths.* **3**, 38–54.

Daly, B. & Harlow, F. 1970 Transport equations in turbulence. *Phys. Fluids* **13**, 2634–2649.

Deardorf, J. 1973 Three-dimensional numerical modeling of the planetary boundary layer. In *Proc. of the Workshop on Micrometeorology*, vol. 271, pp. 271–311. American Meteorological Society.

Dol, H., Hanjalić, K. & Kenjereš, S. 1997 A comparative assessment of the second moment differential and algebraic models in turbulent natural convection. *Intl J. Heat Fluid Flow* **18**, 4–14.

Dol, H., Hanjalić, K. & Versteegh, T. 1999 A DNS-based thermal second-moment closure for buoyant convection at vertical walls. *J. Fluid Mech.* **391**, 211–247.

Elghobashi, S. & Launder, B. 1983 Turbulent time scales and the dissipation rate of temperature variance in the thermal mixing layer. *Phys. Fluids* **26**, 2415–2419.

Grötzbach, G. 1987 Direct numerical and large eddy simulation of turbulent channel flows. In *Encyclopaedia of Fluid Mechanics* (ed. N. Cheremisinoff), vol. 6, pp. 1337–1391. Gulf, Houston.

Hanjalić, K. 1994 Achievements and limitations in modelling and computation of buoyant turbulent flows and heat transfer. In *Proc. Tenth Intl Heat. Transf. Conf.* (ed. G. Hewitt), pp. 1–18. Brighton, UK.

Hanjalić, K. & Launder, B. 1972 A Reynolds stress model of turbulence and its application to thin shear flows. *J. Fluid Mech.* **52**, 609–638.

Hanjalić, K. & Launder, B. 1976 Contribution towards a Reynolds-stress closure for low-Reynolds-number turbulence. *J. Fluid Mech.* **74**, 593–610.

Harari, I. & Hughes, T. 1991 Finite element method for the Helmholtz equation in an exterior domain: model problems. *Comput. Meth. Appl. Mech. Engng.* **87**, 59–96.

Hinze, J. 1975 *Turbulence*, 2nd edn. McGraw-Hill.

Ihlenburg, F. & Babuška, I. 1995 Finite element solution of the Helmholtz equation with high wave number. Part I: the h-version of the FEM. *Comput. Math. Applic.* **30**, 9–37.

Jones, W. & Musonge, P. 1988 Closure of the Reynolds-stress and scalar flux equations. *Phys. Fluids* **31**, 3598–3604.

Jovanović, J., Ye, Q.-Y. & Durst, F. 1995 Statistical interpretation of the turbulent dissipation rate in wall-bounded flows. *J. Fluid Mech.* **293**, 321–347.

Kays, W. 1994 Turbulent Prandtl number – where are we? *J. Heat Transfer* **116**, 284–295.

Knebel, J., Cheng, X., Müller, G., Schumacher, G., Konys, J., Wedemeyer, O., Grötzbach, G. & Carteciano, L. 2001 Thermalhydraulic and material specific investigations into the realization of an accelerator driven system (ADS) to transmute minor actinides. *Tech. Rep.* FZKA 6618. Forschungszentrum Karlsruhe.

Kolovandin, B. & Vatutin, I. 1972 Statistical transfer theory in non-homogeneous turbulence. *Intl J. Heat Mass Transfer* **15**, 2371–2383.

LaRue, J. & Libby, P. 1981 Thermal mixing layer downstream of half heated turbulence grid. *Phys. Fluids* **24**, 597–603.

Launder, B. 1988 On the computation of convective heat transfer in complex turbulent flows. *Trans. ASMEC: J. Heat Transfer* **110**, 1112–1128.

Milionshtchikov, M. 1941 On the theory of homogeneous isotropic turbulence. *CR Acad. Sci. SSSR* **32**, 615–619.

Nagano, Y. & Kim, C. 1988 A two equation model for heat transport in wall turbulent shear flows. *Trans ASMEC: J. Heat Transfer* **110**, 583–589.

Shikazono, N. & Kasagi, N. 1996 Second-moment closure for turbulent scalar transport at various Prandtl numbers. *Intl J. Heat Mass Transfer* **39**, 2977–2987.

Spalding, D. 1971 Concentration fluctuations in a round turbulent free jet. *Chem. Engng. Sci.* **26**, 95–107.

Versteegh, T. & Nieuwstadt, F. 1998 Turbulent budgets of natural convection in an infinite, differentialy heated vertical channel. *Intl J. Heat Fluid Flow* **19**, 135–149.

Wörner, M. 1994 Direkte Simulation turbulenter Rayleigh–Bénard-Konvektion in flüssigem Natrium. PhD thesis, KFK 5228, Forschungszentrum Karlsruhe.

Wörner, M. & Grötzbach, G. 1996*a* Analysis of the transport equation of temperature variance dissipation rate by direct numerical simulation data of natural convection. In *Engineering Turbulence Modelling and Experiments 3* (ed. W. Rodi & G. Bergeles), pp. 229–238. Elsevier.

Wörner, M. & Grötzbach, G. 1996*b* Analysis of thermal variance equation for natural convection of air and sodium. In *Engineering Turbulence Heat and Mass Transfer 1* (ed. K. Hanjalić & M. Pereira), pp. 332–337. Begel House, New York.

Wörner, M., Ye, Q.-Y. & Grötzbach, G. 1999 Consistent modelling of fluctuating temperature-gradient–velocity-gradient correlations for natural convection. In *Engineering Turbulence Modelling and Experiments 4* (ed. W. Rodi & D. Laurence), pp. 165–174. Elsevier.